The Astrophysical Journal, 984:54 (7pp), 2025 May 1 https://doi.org/10.3847/1538-4357/adc44d

An NGC 1068-informed Understanding of Neutrino Emission of the Active Galactic Nucleus TXS 0506+056

Arifa Khatee Zathul, Marjon Moulai, Ke Fang, and Francis Halzen
Department of Physics, Wisconsin IceCube Particle Astrophysics Center, University of Wisconsin–Madison, Madison, WI 53706, USA; arifa@wisc.edu
Received 2024 December 12; revised 2025 March 6; accepted 2025 March 22; published 2025 April 25

Abstract

We present arguments that the neutrinos observed by IceCube from the active galactic nucleus TXS 0506+056 may originate near its core and not in the blazar jet. The origin of the neutrinos is consistent with the mechanism that produces the neutrino flux observed from the active galaxies NGC 1068 and NGC 4151, but requires an Eddington luminosity cosmic-ray flux to compensate for its larger distance. Like NGC 1068, the source is characterized by episodes of high X-ray emission and is gamma-ray-obscured during the 2014 burst, and there is evidence that this is also the case during the short burst in 2017 that produced IC-170922. The observations may be explained as a flux originating in an obscured core within $10 \sim 100$ Schwarzschild radii from the central black hole, which is not transparent to gamma rays from the decay of neutral pions accompanying the neutrinos.

Unified Astronomy Thesaurus concepts: Active galactic nuclei (16); Blazars (164); High energy astrophysics (739); Gamma-rays (637); Cosmic rays (329); Neutrino astronomy (1100); X-ray sources (1822); Seyfert galaxies (1447); Particle astrophysics (96); Black holes (162); Black hole physics (159)

1. Introduction

Understanding the high-energy neutrino emission of the "blazar" TXS 0506+056, the first cosmic-ray accelerator identified in a multimessenger campaign in 2017, has presented an unmet challenge. Guided by its astronomical classification as a BL Lac object,[1] modeling of neutrino production has been focused on the jet. Jets emitting high-energy photons are unlikely to be intense neutrino sources. Transparent to photons, protons, even if accelerated along with electrons, are unlikely to find a target to produce neutrinos since the number of protons available for interaction might be limited due to the jet's low opacity to protons. Detailed modeling has confirmed that matching the neutrino flux level of the 2017 burst is challenging; the origin of the gamma-ray-obscured 2014 burst remains a mystery (see, for instance, M. Cerruti et al. 2019; A. Keivani et al. 2018; N. Sahakyan 2018; S. Gao et al. 2019; P. Padovani et al. 2019; A. Reimer et al. 2019; W. Winter et al. 2019; R. Xue et al. 2019; S. Sahu et al. 2020; G. Cao et al. 2020; B. T. Zhang et al. 2020; W. Jin et al. 2021; V. A. Acciari et al. 2022; S. Das et al. 2022; K. Wang et al. 2022; Z.-J. Wang et al. 2024). While multizone models leveraging a large number of parameters may fit the data, we argue that the mechanism that naturally accommodates the production of neutrinos in the core of the active galaxy NGC 1068 may also contribute to the neutrino production in TXS 0506+056.

A neutrino source requires the acceleration of protons and the presence of a neutrino-producing target. These two requirements may naturally occur close to the black holes at the centers of active galaxies, as underscored by the observation of NGC 1068 (IceCube Collaboration et al. 2022). NGC 1068 is among the brightest nearby active galaxies. Time-integrated searches using IceCube data have identified an excess of high-energy neutrinos from its direction. The energy flux of neutrinos is 1 to 2 orders of magnitude higher than the GeV to TeV gamma-ray flux of this active galaxy, as can be seen in Figure 4 of IceCube Collaboration et al. (2022). This requires a neutrino production site that is opaque to high- and very-high-energy gamma rays, narrowing the possibilities down to the core of the active galaxy (Y. Inoue et al. 2020; K. Murase et al. 2020).

Neutrino production by cosmic-ray accelerators requires a high-density target of photons or protons to produce pions or other particles that are the parents of neutrinos, such as coronal X-rays or regions of large hydrogen density near the cores of active galaxies. Among active galaxies, the intense X-ray emission and large optical depth, $N_{\rm H}$, are likely to be better indicators of neutrino emission than their astronomical classification, though the measurement of these observables may be biased by the orientation of the galaxy.

2. Multimessenger Observations of TXS 0506+056

We briefly summarize here the relevant multimessenger information on TXS 0506+056 before interpreting it in the broad context of the corona model for neutrino production in active galaxies (Y. Inoue et al. 2020; L. A. Anchordoqui et al. 2022; S. Inoue et al. 2021; A. Kheirandish et al. 2021; B. Eichmann et al. 2022; K. Murase 2022; M. Ajello et al. 2023; A. Das et al. 2024a; D. F. G. Fiorillo et al. 2024a, 2024b; R. Mbarek et al. 2024) inspired by the observations of NGC 1068. On 2017 September 22, IceCube reported a well-reconstructed muon that deposited 180 TeV inside the detector, corresponding to a most probable energy of 290 TeV (C. Kopper & E. Blaufuss 2017; IceCube Collaboration et al. 2018) for the parent neutrino, known as IC-170922A. Its arrival direction was aligned with the coordinates of a known Fermi blazar, TXS 0506+056, to within $0.^{\circ}06$. The source was "flaring" with a gamma-ray flux that had increased by a factor of 7 in recent months. A variety of estimates converged on a probability on the order of 10^{-3} that the coincidence was accidental (C. Kopper & E. Blaufuss 2017;

[1] Though this classification is under debate. P. Padovani et al. (2019) suggest that TXS 0506+056 is not a blazar of the BL Lac type but instead is intrinsically a flat-spectrum radio quasar.

IceCube Collaboration et al. 2018). The identification of the neutrino with the source reached the level of evidence, but not more. What clinched the association was a series of subsequent observations, culminating with a significant optical flux variation associated with IC-170922A (V. Lipunov et al. 2020), conclusively associating the neutrino with TXS 0506+056. Searching the archival IceCube data revealed that the neutrino luminosity of TXS 0506+056 is dominated by a burst observed in 2014–2015 (M. Aartsen et al. 2018), which leaves the burst associated with IC 170922 as a subdominant contribution.

The sequence of observations relevant to this paper can be summarized as follows.

1. The redshift of the host galaxy was measured to be $z \simeq 0.34$ (S. Paiano et al. 2018). It is important to realize that nearby blazars like the Markarian sources are at a distance that is 10 times closer, and therefore TXS 0506 +056, with a similar gamma-ray flux despite its greater distance, is one of the most luminous sources in the Universe. This suggests that it belongs to a special class of sources that accelerate proton beams inside dense environments, as revealed by the neutrino.
2. Originally detected by NASA's Swift (P. Evans et al. 2017) and Fermi (Y. T. Tanaka et al. 2017) satellites, the neutrino alert was followed up by ground-based air Cherenkov telescopes (R. Mirzoyan et al. 2017). MAGIC detected the emission of gamma rays with energies exceeding 100 GeV starting several days after the observation of IC-170922A (S. Ansoldi et al. 2018). Given its distance, this establishes the source as a relatively rare TeV blazar.
3. Informed on where to look, IceCube searched its archival neutrino data up to and including 2017 October for evidence of neutrino emission at the location of TXS 0506+056. IceCube found 19 high-energy neutrino events in 2014–2015 on a background of fewer than six in a burst that lasted 110 days (M. Aartsen et al. 2018). This burst dominates the integrated flux from the source over the last 9.5 yr of archival IceCube data, leaving the 2017 burst as a second subdominant feature.
4. The MASTER robotic optical telescope network, which had been monitoring the source since 2005, found its strongest time variation in the last 15 yr to have occurred 2 hr after the emission of IC-170922, with a second, less statistically compelling variation following the 2014 burst (V. Lipunov et al. 2020). The source switches from the "off" to the "on" state 2 hr after the emission of the neutrino. After monitoring the uniformity of their observations until the first quarter of 2020, they concluded that the time variation detected on 2017 September 22 is at a level of 50σ, which conclusively associates the source with the neutrino. Such strong variability may be caused by changes in the accretion rate of the central engine (C. Ricci & B. Trakhtenbrot 2023).
5. Using 10 years of IceCube data collected between 2008 April 6 and 2018 July 10, a search for pointlike sources found TXS 0506+056 as the second most significant source, after NGC 1068, in IceCube's northern source catalog (M. G. Aartsen et al. 2020). The signal in the direction of TXS 0506+056 integrated over 10 years has a pretrial significance of 3.6σ.

Additionally, it is important to note that the high-energy neutrino spectra covering the 2014 burst as well as the 10 yr time-integrated search are consistent with a hard $\sim E^{-2}$ spectrum, which is expected for a cosmic accelerator.

In what follows, the motivation for a common origin of high-energy neutrinos from NGC 1068 and TXS 0506+056 will be mostly based on their high X-ray fluxes, but also on the fact that gamma-ray observations do not show evidence for the gamma-ray emission from the decay of the accompanying neutral pions, as we will argue further on. This should anyway not come as a surprise because the obscuration of pionic gamma rays is also the case for other sources that have reached the level of evidence in the IceCube data (R. Abbasi et al. 2024a, 2025). The high level of the diffuse neutrino flux observed by IceCube relative to the diffuse gamma-ray flux measured by the Fermi satellite indicates that typical neutrino sources are gamma-ray-obscured sources (K. Murase et al. 2016; K. Fang et al. 2022). Where TXS 0506+056 is concerned, the dominant flare observed in 2014 is not accompanied by an elevated gamma-ray flux. What about the "flaring" blazar in 2017? Although the source had been flaring for several months, the Fermi data indicate a minimum of the flux at the time IC-170922 was emitted; for a discussion, see E. Kun et al. (2021), with a hint that the source may have been gamma-ray-obscured over a short period, possibly hours, as indicated by the optical observation. In this paper, we will argue that the neutrinos are produced in the core of TXS 0506 +056, which provides an appropriate environment for accelerating protons and converting them to neutrinos, as is the case in NGC 1068.

Like many other blazars, the spectral energy distribution of TXS 0506+056 presents two emission peaks. The lower one peaking in the optical band extending to soft X-ray may be explained as synchrotron radiation by relativistic electrons from the jet. The second peak at gamma-ray energies is usually interpreted as the synchrotron-self-Compton emission by the same jet electrons or, in a hadronic scenario, as the electromagnetic cascades from photopion or Bethe–Heitler interactions of cosmic-ray protons from the jet (see, for example, A. Keivani et al. 2018). On the other hand, recent observations of blazar outbursts have identified an additional component in the X-ray spectrum extending well above 10 keV, which could represent a temporarily enhanced emission from an accretion disk corona (K. K. Madsen et al. 2015; E. Prandini & G. Ghisellini 2022). Moreover, studies have shown that the X-ray emission in many radio-loud active galactic nuclei (AGN) appears to come from a corona, rather than from the jet (S. F. Zhu et al. 2020). The coronal X-ray emission from AGN is highly variable with flares on a timescale of hours, reaching 100 keV and higher energies (e.g., P. Rani et al. 2019; R. Serafinelli et al. 2024). Hard X-ray emission from TXS 0506+056 was detected by NuSTAR in two Target of Opportunity observations following IC-170922, but was not measured during the 2014 flare.

Inspired by the blazar outburst observations, we argue that the corona of TXS 0506+056 may also partly contribute to the X-ray emission, which is at the level of $L_X \sim 9 \times 10^{44}\,\mathrm{erg\,s^{-1}}$ at ∼15–55 keV (A. Keivani et al. 2018; E. Kun et al. 2024). Such a coronal component allows an alternative explanation for the origin of the detected neutrinos, implying that they may arise from the core instead of the jets. Importantly, the coronal power may exceed the source luminosity due to gas absorption,

which is particularly observed in the soft X-ray band (R. C. Hickox & D. M. Alexander 2018).

We will show that the neutrino flux observed from TXS 0506+056 can be accommodated assuming a core with characteristic photon densities that are similar to those in NGC 1068. The source does require a proton flux increased to super-Eddington level during the neutrino flaring time in order to accommodate a neutrino flux similar to that of NGC 1068 for a source at a larger distance. The model also assumes that most of the observed X-ray emission originates from the corona and not the jet.

3. Corona-disk Model

A corona is a dense X-ray emitting region that surrounds the black hole. Assuming a spherical geometry with a radius R, the energy density of the X-rays associated with the corona, u_X, is related to the X-ray luminosity, L_X, of the source by

$$u_X = \frac{L_X}{4\pi c R^2} \approx n_X E_X, \tag{1}$$

where L_X is the X-ray luminosity measured at energy E_X, c is the speed of light, and $n_X \approx u_X/E_X$ is the number density of X-rays in the target. Protons accelerated near the black hole interact with the X-ray photons to produce neutrinos.

Protons may be accelerated in turbulence or collisionless magnetic reconnection in the coronal region. The coronal magnetic field, B, may be estimated by $u_B = B^2/8\pi = \xi_B u_X$, where u_B is the magnetic energy density and ξ_B is the conversion factor between radiation and magnetic energy density that is on the order of unity. The maximum attainable energy for protons is $E \sim eBR = e(2L_X/\xi_B c)^{1/2}$, sufficient to produce the TeV–PeV neutrinos. The actual maximum proton energy and the spectrum depend on the acceleration mechanism. In a scenario where protons obtain their energies by stochastic scattering on the turbulent fluctuations, particles may be efficiently confined by the magnetic fields before cooling (K. Murase et al. 2020; R. Mbarek et al. 2024; D. F. G. Fiorillo et al. 2024b). In a scenario where protons are accelerated by magnetic reconnection, the short acceleration process competes with a fast escape of the particles from the reconnection layer (D. F. G. Fiorillo et al. 2024b). A two-step acceleration process where particles get preaccelerated before arriving at the corona may also be present (R. Mbarek et al. 2024).

Relativistic protons leave the acceleration region by diffusing away from the turbulent magnetic field or being advected toward the black hole. The fallback time is $t_{\rm fall} = R/\alpha v_K$, where $\alpha \sim 0.1$ is the viscous parameter and $v_K = (GM/R)^{1/2}$ is the disk velocity in circular Keplerian orbits (N. I. Shakura & R. A. Sunyaev 1973). The diffusion time, $t_{\rm diff}$, depends on the strength and properties of the magnetic field. In general, $t_{\rm fall}$ is shorter than $t_{\rm diff}$ at lower energies and longer than $t_{\rm diff}$ at higher energies. As in S. I. Stathopoulos et al. (2024) and S. Das et al. (2024b), we assume that the escape time of charged particles is a constant factor of the light-crossing time, $t_{\rm esc} = (c/v_{\rm esc})\,(R/c)$, where the ratio between the light speed and the escape speed of charged particles is $c/v_{\rm esc} = 10$–100.

The critical quantity for neutrino production is the proton's opacity for interacting in the corona. It determines the number of pions that decay into neutrinos and gamma rays:

$$\tau_{p\gamma} = \kappa_{p\gamma}\frac{ct_{\rm esc}}{\lambda_{p\gamma}} \approx n_X \kappa_{p\gamma}\sigma_{p\gamma} ct_{\rm esc} \approx \frac{u_X}{E_X}\kappa_{p\gamma}\sigma_{p\gamma} ct_{\rm esc}. \tag{2}$$

We will assume that the pions are produced on the Δ resonance with inelasticity $\kappa_{p\gamma} \equiv E_\pi/E_p \simeq 0.2$, which encodes the amount of energy transferred from protons to pions (π^0 or π^+) in each interaction. $\lambda_{p\gamma}$ is the interaction length, which is inversely proportional to the density of the target, n_X, and to the photoproduction cross section, $\sigma_{p\gamma} \simeq 5 \times 10^{-28}\,{\rm cm}^2$. The optical depth can be rewritten in terms of the Eddington luminosity, $L_{\rm edd}$, and the Schwarzschild radius, R_S, of the black hole of mass M:

$$\begin{aligned}\tau_{p\gamma} &= \frac{\kappa_{p\gamma}\sigma_{p\gamma}}{4\pi c}\left(\frac{c}{v_{\rm esc}}\right)\frac{1}{R}\frac{L_X}{E_X} \\ &\simeq 70\left(\frac{v_{\rm esc}}{c}\right)^{-1}\left(\frac{R}{R_s}\right)^{-1}\left(\frac{E_X}{1\,{\rm keV}}\right)^{-1}\left(\frac{L_X}{L_{\rm edd}}\right),\end{aligned} \tag{3}$$

where $L_{\rm edd} = 1.26 \times 10^{38}\,(M/M_\odot)\,{\rm erg\,s^{-1}}$ and $R_s = 2GM/c^2 = 3 \times 10^5\,M/M_\odot\,{\rm cm}$.

In what follows we estimate the opacity using the X-ray flux at a typical energy of 1 keV, which lies within the soft X-ray energy band of 0.3–10 keV. The information on both sources that will be used as input into our modeling is summarized in Table 1. Given the challenges in isolating the coronal X-ray flux contribution from the observed flux and the need to assign a neutrino flux to TXS 0506+056 based on only two observed neutrino flares, we have assigned generous uncertainties to the input quantities. Note that the uncertainties in the distance d_L and Schwarzschild radius R_s in Table 1 are not accounted for in the calculations. The error propagation is done by separately summing the upper and lower errors in quadrature.

NGC 1068 has a black hole mass of $1.3^{+1.7}_{-0.6} \times 10^7\ M_\odot$ (L. Greenhill & C. Gwinn 1997; J. Kamenetzky et al. 2011; J.-M. Wang et al. 2020; P. Padovani et al. 2024), corresponding to an Eddington luminosity of $L_{\rm edd} = 1.6^{+2.1}_{-0.8} \times 10^{45}\,{\rm erg\,s^{-1}}$. The intrinsic X-ray luminosity is reported to be (3–7) $\times 10^{43}\,{\rm erg\,s^{-1}}$ (F. E. Bauer et al. 2015; A. Marinucci et al. 2015; P. Padovani et al. 2024) in the 2–10 keV band. For a consistent comparison with the X-ray luminosity of TXS 0506+056, we extrapolate the

Table 1
Input Values for Modeling and Calculating the Opacities and the Proton Luminosities of NGC 1068 and TXS 0506+056

Parameter	NGC 1068	TXS 0506+056
Mass, M $(M_\odot)$	$1.3^{+4.3}_{-0.6} \times 10^7$	$3.1^{+29.9}_{-2.7} \times 10^8$
Schwarzschild radius, $R_{S\ ({\rm cm})}$	$3.9^{+5.1}_{-1.8} \times 10^{12}$	$9.3^{+71.1}_{-8.2} \times 10^{12}$
Luminosity distance, $d_{L\ ({\rm Mpc})}$	$14.4^{+2.1}_{-7.2}$	1774^{+63}_{-24}
Eddington luminosity, $L_{\rm edd}$ (erg s^{-1})	$1.6^{+2.1}_{-0.8} \times 10^{45}$	$3.9^{+29.9}_{-3.4} \times 10^{46}$
Neutrino luminosity, L_ν (erg s^{-1})	$2.9^{+1.4}_{-2.4} \times 10^{42}$	$6.8^{+4.4}_{-3.6} \times 10^{45}$ (9.5 yr duration), $1.1^{+0.5}_{-0.4} \times 10^{47}$ (158 days duration)
X-ray luminosity, L_X (erg s^{-1})	$2.2^{+0.4}_{-1.7} \times 10^{43}$	$8.5^{+2.0}_{-4.8} \times 10^{44}$
X-ray energy, E_X (keV)	1	1

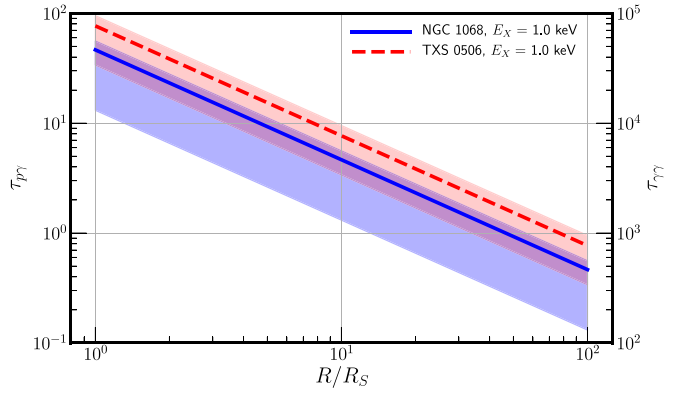

Figure 1. Photopion opacities against emission radii for NGC 1068 (blue solid line) and TXS 0506 (red dashed line) computed using Equation (2).

2–10 keV flux to a broader 0.3–10 keV X-ray band. By normalizing the intrinsic X-ray flux $F^{\rm intr}_{X,\,2-10\,{\rm keV}} = 2.7 \times 10^{-10}$ erg cm^{-2} s^{-1} from the latest BASS catalog (C. Ricci et al. 2017) and assuming a power-law spectral index of $\gamma_X = 2.4^{+0.1}_{-0.1}$ based on the torus model, we obtain an intrinsic X-ray flux and luminosity of $F^{\rm intr}_{X,\,0.3-10\,{\rm keV}} = 8.8^{+0.1}_{-0.8} \times 10^{-10}$ erg cm^{-2} s^{-1}. This corresponds to $L^{\rm intr}_{X,\,0.3-10\,{\rm keV}} = 2.2^{+0.4}_{-1.7} \times 10^{43}$ erg s^{-1} for a source distance of 14.4 Mpc (L. Bottinelli et al. 1997; J. Bland-Hawthorn et al. 1997; GRAVITY Collaboration et al. 2019).

The resulting opacity for $p\gamma$ interactions is shown in Figure 1. The value of $\tau_{p\gamma} \sim 1$ for $R/R_S \sim 10$ reproduces the value obtained by more detailed modeling in the context of the core corona model (K. Murase 2022). This dimensional analysis of NGC 1068 underscores the fact that the production of the neutrinos inside a dense X-ray core naturally reaches the level of neutrino production observed by IceCube. With $\tau_{\gamma\gamma} \sim 10^3 \times \tau_{p\gamma}$, as shown in Figure 1, the gamma rays from the decay of neutral pions accompanying the neutrinos lose energy in the corona by pair production with the X-ray photons. The suppression accommodates the upper limits established by MAGIC (V. A. Acciari et al. 2019), which limits their TeV gamma-ray flux to 2 orders of magnitude below the neutrino flux at some energies.

The core of NGC 1068 not only hosts a dense X-ray corona but also dense clouds of hydrogen, identified by large values of N_H along the line of sight (S. Garcìa-Burillo et al. 2016; V. G. Rosas et al. 2022). The proton opacity due to interaction with the gas depends on the composition of the corona. If the proton energy density is comparable to or larger than the electron energy density in the corona, and if $\tau_{pp} \sim 1$, then neutrinos may actually be predominantly produced by pp interactions. Even if this is the case, the large value of $\tau_{p\gamma}$ is still required to absorb the gamma rays produced by the π^0 photons accompanying the observed neutrino flux.

Applying the same dimensional analysis to TXS 0506+056 results in similar opacity values as shown in Figure 1. The literature agrees on a black hole mass of approximately 3×10^8 $M_\odot$ (P. Padovani et al. 2019; J. B. Tjus et al. 2022). In this work, we adopt the approach described in P. Padovani et al. (2019) to infer the black hole mass with uncertainties. Taking the absolute R-band magnitude of the bulge to be -22.9, and using the active galactic black hole mass–bulge luminosity relation from R. J. McLure & J. Dunlop (2002), we obtain a mass of $3.1^{+29.9}_{-2.7} \times 10^8$ $M_\odot$. This result is consistent with the previous estimate, and it corresponds to an Eddington luminosity of $L_{\rm edd} = 3.9^{+29.9}_{-3.4} \times 10^{46}$ erg s^{-1}. To derive the X-ray luminosity, we adopt Swift's X-Ray Telescope's (Swift-XRT) flux observation of $F_{X,\,0.3-10\,{\rm keV}} = 2.3^{+0.5}_{-1.3} \times 10^{-12}$ erg cm^{-2} s^{-1} in the 0.3–10 keV band, which represents the mean flux when the source was in its flaring state (A. Keivani et al. 2018). Note that the observed X-ray flux of TXS 0506+056 serves as a lower limit to the intrinsic X-ray flux of the source, which includes contributions from the coronal, the jet, and other possible X-ray emitting components. The intrinsic flux of the coronal region alone is rather unknown below 10 keV. Assuming that it is comparable to this observed flux, we obtain an X-ray luminosity of $L^{\rm intr}_{X,\,0.3-10\,{\rm keV}} = 8.5^{+2.0}_{-4.8} \times 10^{44}$ erg s^{-1} assuming a source luminosity distance of $d_L = 1774$ Mpc (S. Paiano et al. 2018). As shown in Figure 1, a value of $\tau_{p\gamma} \sim 10$ is also found for $R/R_S \sim 10$, which decreases to 1 for $R/R_S \sim 100$.

Next, we compute the proton emissivity Q_p required to generate the observed neutrino emissivities, Q_ν, in a target with opacity $\tau_{p\gamma}$:

$$E_\nu^2 Q_\nu \approx \frac{3}{8} f_{p\gamma} E_p^2 Q_p, \tag{4}$$

where

$$f_{p\gamma} \equiv 1 - e^{-\tau_{p\gamma}} \tag{5}$$

is the pion production efficiency. In this equation, the differential neutrino luminosity $L_\nu = E_\nu^2 Q_\nu$ includes the three neutrino flavors.

At large neutrino emission radii $R \gg R_s$ and small opacity limit $\tau_{p\gamma} \ll 1$, Equation (4) yields

$$\begin{aligned} L_\nu &\approx \frac{\kappa_{p\gamma}\sigma_{p\gamma}}{4\pi v_{\rm esc}} \frac{L_p}{R E_X} L_X \\ &= 0.7 \left(\frac{v_{\rm esc}}{0.1\,c}\right)^{-1} \left(\frac{L_p}{10^{-2}\,L_{\rm edd}}\right) \left(\frac{R}{10\,R_s}\right)^{-1} \left(\frac{E_X}{1\,{\rm keV}}\right)^{-1} L_X. \end{aligned} \tag{6}$$

In Figure 2, we compare Equation (6) with observations of sources assuming that they produce steady neutrino emission. For NGC 4151 (M. C. Bentz & S. Katz 2015; W. Yuan et al. 2020; M. C. Bentz et al. 2022; Y. Inoue & D. Khangulyan 2023), we calculated the neutrino luminosity using the flux and spectral index reported in R. Abbasi et al. (2025), while the X-ray flux is determined using the same methodology as for NGC 1068, with parameters obtained from C. Ricci et al. (2017). Figure 2 indicates that the previously discussed analysis would also apply to the case of NGC 4151, and TXS 0506 could belong to the group within the uncertainties. E. Kun et al. (2024) and A. Neronov et al. (2024) have also argued for a neutrino luminosity that is proportional to the X-ray luminosity with a coefficient of order unity.

In the large opacity limit $\tau_{p\gamma} \gg 1$, the exponential term gets suppressed, and we are left with a neutrino luminosity that scales linearly with proton luminosity,

$$L_\nu \sim \frac{3}{8} L_p. \tag{7}$$

For NGC 1068, the all-flavor neutrino flux is $\phi_0 = (15.0 \pm 6.3) \times 10^{-11}$ TeV^{-1} cm^{-2} s^{-1} at 1 TeV with a spectral index of $\gamma = 3.2 \pm 0.2$ (IceCube Collaboration et al. 2022). Integrating the flux between neutrino energies of 1.5 and 15 TeV (IceCube Collaboration et al. 2022) yields a neutrino luminosity of $L_\nu = 2.9^{+1.4}_{-2.4} \times 10^{42}$ erg s^{-1}. To produce such a neutrino flux, a proton luminosity of $L_p = 7.7^{+3.6}_{-6.4} \times 10^{42}$ erg s^{-1}

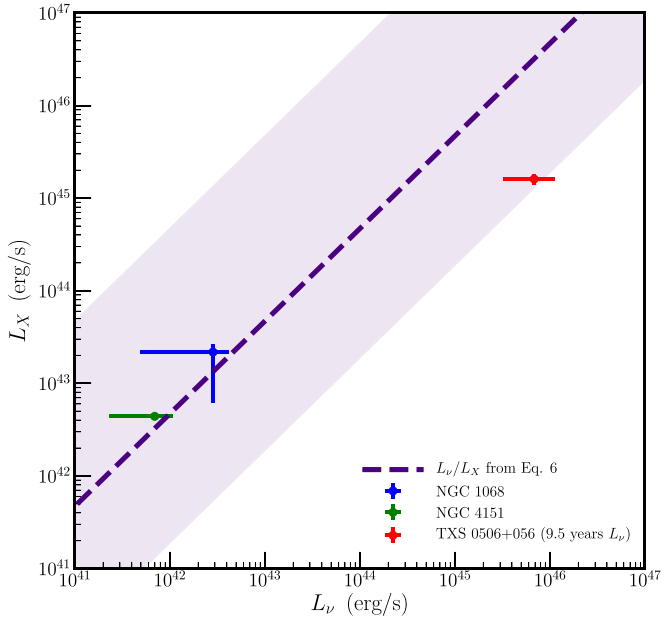

Figure 2. Plot showing the X-ray and neutrino luminosities for sources in steady emission states, namely NGC 1068 (blue), TXS 0506+056 (red), and NGC 4151 (green). The red point is plotted using the neutrino luminosity computed using the 9.5 yr of IceCube data and the NuSTAR X-ray fluxes reported in A. Keivani et al. (2018). The purple line shows the linear relationship between L_ν and L_X derived in Equation (6), and the purple shaded region encodes the propagated errors associated with the slope, where we took the ranges of input parameters $L_p/L_{\rm edd}$ to be between 10^{-3} and 1, and R/R_S to be between 10 and 100.

is required, assuming a neutrino emission radius of $R/R_S = 10^{+90}_{-9}$.

For TXS 0506+056, a 9.5 yr time-integrated neutrino flux of $\Phi_{\nu_\mu} = 0.8^{+0.5}_{-0.4} \times 10^{-16}$ TeV^{-1} cm^{-2} s^{-1} normalized at 100 TeV and a spectral index of $\gamma = 2.0 \pm 0.3$ at 100 TeV (IceCube Collaboration et al. 2018) corresponds to a neutrino luminosity of $L_{\nu_\mu} = 2.3^{+1.5}_{-1.2} \times 10^{45}$ erg s^{-1} between 32 TeV and 3.6 PeV. At the same neutrino emission radius of $R/R_S = 10^{+90}_{-9}$, a proton luminosity of $L_p = 1.8^{+1.2}_{-1.0} \times 10^{46}$ erg s^{-1} is needed, assuming that the neutrino emission is isotropic over a 4π solid angle. Alternatively, we could use the 158 day neutrino flux (observed in 2014) of $\Phi_{\nu_\mu} = 1.6^{+0.7}_{-0.6} \times 10^{-15}$ TeV^{-1} cm^{-2} s^{-1} normalized at 100 TeV with a spectral index of $\gamma = 2.2 \pm 0.2$ (IceCube Collaboration et al. 2018). This corresponds to a neutrino luminosity of $L_{\nu_\mu} = 3.7^{+1.7}_{-1.4} \times 10^{46}$ erg s^{-1} when integrated between 32 TeV and 3.6 PeV and a proton luminosity of $L_p = 3.0^{+1.3}_{-1.1} \times 10^{47}$ erg s^{-1}.

The proton luminosities for emission radii between $R/R_S = 1$–100 are shown in Figure 3 for NGC 1068 (blue solid line) and TXS 0506+056 (red dashed and brown loosely dashed lines). Note that while the proton luminosity is well below the Eddington limit for NGC 1068, to explain the time-integrated flux of TXS 0506+056, $L_p \sim 20\,L_X$ is needed. To explain the flares of TXS 0506+056, it requires the presence of a corona with super-Eddington-level power. This is a challenging condition to meet, requiring scenarios where the corona power is dominated by relativistic protons and a super-Eddington activity that occurred around the time of IC-170922. Such models have been explored in the context of magnetically arrested disk states, for example in K. Hayasaki & R. Yamazaki (2019) and Q.-R. Yang et al. (2025). Alternatively, if one

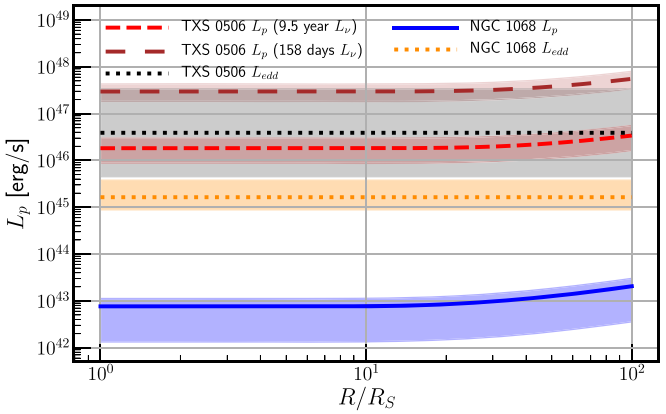

Figure 3. Plot of proton and Eddington luminosities against emission radii for NGC 1068 (blue solid and orange dotted lines) and TXS 0506+056 (red dashed, brown loosely dashed, and black dotted lines). The red dashed and brown loosely dashed lines denote the proton luminosities computed using 9.5 yr and 158 days of neutrino data, respectively.

constrains the proton luminosity by $L_p \lesssim L_X$, our model predicts that the corona of TXS 0506+056 may power a neutrino luminosity up to $L_\nu \sim 3.4 \times 10^{44}$ erg s^{-1}, which is lower than what was observed.

In Figures 2 and 3, L_ν and L_p are calculated from the observed neutrino flux, which spans slightly different energy ranges in these two sources. The proton spectrum in a corona depends on the acceleration mechanism and on the properties of the emission site, such as the magnetization (e.g., K. Fang et al. 2024). Consequently, detailed modeling is required to determine L_p, especially beyond the energy range where neutrinos are observed.

4. Conclusion

In this paper we have shown that the first high-energy neutrino sources observed by IceCube are active galaxies, which is consistent with the observation that our own Galaxy does not dominate the neutrino sky. With the neutrinos produced in the dense core near the supermassive black hole, they are also obscured in gamma rays, as expected from the fact that Fermi does not observe the gamma rays of neutral pion origin accompanying the diffuse neutrino flux. The presence of an X-ray corona is essential to absorb the gamma rays to the low gamma-ray flux levels observed. Our analysis meets the challenge of modeling the TXS 0506+056 multimessenger spectrum with the same mechanism derived from the multi-messenger observations of NGC 1068 and NGC 4151.

This observation raises the possibility that such sources represent generic sources where extragalactic cosmic rays originate. The relation (M. Ahlers & F. Halzen 2014) connecting the flux of the nearest source with neutrino flux L_ν to the total diffuse flux Φ_ν from a uniform distribution of sources with a density $\rho(z)$ in the Universe is given by

$$E_\nu^2 \Phi_\nu^{\rm diff} = \frac{1}{4\pi} \frac{c}{H_0} \xi_z \, \rho L_\nu, \tag{8}$$

where H_0 is the Hubble parameter and ξ_z the result of integration over the redshift of the sources, which reduces to an overall factor assuming that the fluxes follow a power law; for instance, $\xi_z \simeq 0.5$ for no source evolution or $\xi_z \simeq 2.6$ for star formation evolution (H. Yüksel et al. 2008). For the value of the diffuse astrophysical neutrino flux observed by IceCube

with $\Phi_{\nu}^{\rm Astro} = 5.04 \times 10^{-11}\,{\rm TeV}^{-1}\,{\rm cm}^{-2}\,{\rm s}^{-1}\,{\rm sr}^{-1}$ at 100 TeV (R. Abbasi et al. 2024b), we find that the local source density of NGC 1068-like and TXS 0506+056-like sources is $\rho_0 = 1.0 \times 10^{-6}$ and $\rho_0 = 1.5 \times 10^{-9}\,{\rm Mpc}^{-3}$ ($\rho_0 = 2.0 \times 10^{-7}$ and $\rho_0 = 2.8 \times 10^{-10}\,{\rm Mpc}^{-3}$), respectively, assuming star formation evolution (no source evolution). With densities $\rho_0 \sim 10^{-6}\,{\rm Mpc}^{-3}$ for NGC 1068-like sources, the diffuse flux is accommodated by $\sim 10^3$ sources, which also happens to be the number of sources in the Universe with X-ray luminosity in excess of $10^{43}\,{\rm erg\,s}^{-1}$ (C. M. Urry & P. Padovani 1995). For an episodic source like TXS 0506+056, the fraction of the time is not known for which it contributes at the high level of the Eddington-level 100 day 2014 burst, which dominates the total emission in the decade that IceCube has observed the source. With an on time of 5%, the density of the sources matches that of NGC 1068 (F. Halzen et al. 2019).

In this context, it is also intriguing that with $\tau_{p\gamma}$ values of order unity for both sources, the diffuse neutrino flux matches the total energy loss $\rho_p L_p \sim 10^{44}\,{\rm erg\,Mpc}^{-3}\,{\rm yr}^{-1}$ of ultrahigh-energy cosmic rays in the Universe (B. Katz et al. 2013) measured by the Auger experiment and Telescope Array.

As already indicated by the observations of NGC 1068, it is possible that neutrinos are not only produced in the X-ray corona but also on the high hydrogen density near the core, and possibly on UV photons associated with the accretion disk. However, the key point is that even in the presence of additional contributions to the neutrino flux, the presence of the corona is essential for absorbing the pionic gamma rays, which are not observed or suppressed at GeV–TeV energies. Such suppression cannot be achieved by the other targets. We emphasize the importance of the X-ray flux in selecting potential neutrino sources, a tool that has already been successfully explored by IceCube to find evidence for more sources (R. Abbasi et al. 2024a, 2025).

Acknowledgments

This work is supported by the Office of the Vice Chancellor for Research at the University of Wisconsin–Madison with funding from the Wisconsin Alumni Research Foundation. K. F. acknowledges support from the National Science Foundation (PHY-2238916). This work was supported by a grant from the Simons Foundation (00001470, K.F.). K.F. acknowledges the support of the Sloan Research Fellowship. The research of F.H. was also supported in part by the US National Science Foundation under grants PHY-2209445 and OPP-2042807 and by the Balzan Foundation.

ORCID iDs

Arifa Khatee Zathul https://orcid.org/0000-0002-8735-8579
Marjon Moulai https://orcid.org/0000-0001-7909-5812
Ke Fang https://orcid.org/0000-0002-5387-8138
Francis Halzen https://orcid.org/0000-0001-6224-2417

References

Aartsen, M., Ackermann, M., Adams, J., et al. 2018, Sci, 361, eaat1378
Aartsen, M. G., Ackermann, M., Adams, J., et al. 2020, PhRvL, 124, 051103
Abbasi, R., Ackermann, M., Adams, J., et al. 2024a, arXiv:2406.07601
Abbasi, R., Ackermann, M., Adams, J., et al. 2024b, PhRvD, 110, 022001
Abbasi, R., Ackermann, M., Adams, J., et al. 2025, ApJ, 981, 131
Acciari, V. A., Ansoldi, S., Antonelli, L., et al. 2019, ApJ, 883, 135
Acciari, V. A., Aniello, T., Ansoldi, S., et al. 2022, ApJ, 927, 197
Ahlers, M., & Halzen, F. 2014, PhRvD, 90, 043005
Ajello, M., Murase, K., & McDaniel, A. 2023, ApJ, 954, L49
Anchordoqui, L. A., Krizmanic, J. F., & Stecker, F. W. 2022, ICRC, 37, 993
Ansoldi, S., Antonelli, L. A., Arcaro, C., et al. 2018, ApJL, 863, L10
Bauer, F. E., Arévalo, P., Walton, D. J., et al. 2015, ApJ, 812, 116
Bentz, M. C., & Katz, S. 2015, PASP, 127, 67
Bentz, M. C., Williams, P. R., & Treu, T. 2022, ApJ, 934, 168
Bland-Hawthorn, J., Gallimore, J., Tacconi, L., et al. 1997, Ap&SS, 248, 9
Bottinelli, L., Gouguenheim, L., Paturel, G., & Teerikorpi, P. 1997, Ap&SS, 248, 9
Cao, G., Yang, C., Yang, J., & Wang, J. 2020, PASJ, 72, 20
Cerruti, M., Zech, A., Boisson, C., et al. 2019, MNRAS, 483, L12
Das, A., Zhang, B. T., & Murase, K. 2024a, ApJ, 972, 44
Das, S., Carpio, J. A., & Murase, K. 2024b, arXiv:2405.06382
Das, S., Gupta, N., & Razzaque, S. 2022, A&A, 668, A146
Eichmann, B., Oikonomou Oikonomou, F., Salvatore, S., Dettmar, R.-J., & Becker Tjus, J. 2022, ApJ, 939, 43
Evans, P., Keivani, A., Kennea, J., et al. 2017, ATel, 10792, 1
Fang, K., Gallagher, J. S., & Halzen, F. 2022, ApJ, 933, 190
Fang, K., Halzen, F., Heinz, S., & Gallagher, J. S. 2024, ApJL, 975, L35
Fiorillo, D. F. G., Comisso, L., Peretti, E., Petropoulou, M., & Sironi, L. 2024a, ApJ, 974, 75
Fiorillo, D. F. G., Petropoulou, M., Comisso, L., Peretti, E., & Sironi, L. 2024b, ApJL, 961, L14
Gao, S., Fedynitch, A., Winter, W., & Pohl, M. 2019, NatAs, 3, 88
Garcìa-Burillo, S., Combes, F., Ramos Almeida, C., et al. 2016, ApJL, 823, L12
GRAVITY Collaboration, Abuter, R., Accardo, M., et al. 2019, Msngr, 178, 20
Greenhill, L., & Gwinn, C. 1997, Ap&SS, 248, 261
Halzen, F., Kheirandish, A., Weisgarber, T., & Wakely, S. P. 2019, ApJL, 874, L9
Hayasaki, K., & Yamazaki, R. 2019, ApJ, 886, 114
Hickox, R. C., & Alexander, D. M. 2018, ARA&A, 56, 625
IceCube Collaboration, Abbasi, R., Ackermann, M., et al. 2022, Sci, 378, 538
IceCube CollaborationMAGICAGILE, et al. 2018, Sci, 361, eaat1378
Inoue, S., Cerruti, M., Murase, K., & Liu, R.-Y. 2021, in ICRC2021 (Trieste: Sissa), 1013
Inoue, Y., & Khangulyan, D. 2023, PASJ, 75, L33
Inoue, Y., Khangulyan, D., & Doi, A. 2020, ApJL, 891, L33
Jin, W., Sharpe, R., Capasso, M., et al. 2021, in Proc. 37th International Cosmic Ray Conf. PoS (ICRC2021) (Trieste: Sissa Medialab), 945
Kamenetzky, J., Glenn, J., Maloney, P., et al. 2011, ApJ, 731, 83
Katz, B., Waxman, E., Thompson, T., & Loeb, A. 2013, arXiv:1311.0287
Keivani, A., Murase, K., Petropoulou, M., et al. 2018, ApJ, 864, 84
Kheirandish, A., Murase, K., & Kimura, S. S. 2021, ApJ, 922, 45
Kopper, C., & Blaufuss, E. 2017, GCN, 21916, 1
Kun, E., Bartos, I., Tjus, J. B., et al. 2024, PhRvD, 110, 123014
Kun, E., Bartos, I., Tjus, J. B., et al. 2021, ApJL, 911, L18
Lipunov, V., Kornilov, V., Zhirkov, K., et al. 2020, ApJL, 896, L19
Madsen, K. K., Fürst, F., Walton, D. J., et al. 2015, ApJ, 812, 14
Marinucci, A., Bianchi, S., Matt, G., et al. 2015, MNRAS, 456, L94
Mbarek, R., Philippov, A., Chernoglazov, A., Levinson, A., & Mushotzky, R. 2024, PhRvD, 109, L101306
McLure, R. J., & Dunlop, J. 2002, MNRAS, 331, 795
Mirzoyan, R., Babić, A., Dominis Prester, D., et al. 2017, ATel, 10817, 1
Murase, K. 2022, ApJL, 941, L17
Murase, K., Guetta, D., & Ahlers, M. 2016, PhRvL, 116, 071101
Murase, K., Kimura, S. S., & Meszaros, P. 2020, PhRvL, 125, 011101
Neronov, A., Savchenko, D., & Semikoz, D. 2024, PhRvL, 132, 101002
Padovani, P., Oikonomou, F., Petropoulou, M., Giommi, P., & Resconi, E. 2019, MNRAS, 484, L104
Padovani, P., Resconi, E., Ajello, M., et al. 2024, NatAs, 8, 1077
Paiano, S., Falomo, R., Treves, A., & Scarpa, R. 2018, ApJL, 854, L32
Prandini, E., & Ghisellini, G. 2022, Galax, 10, 35
Rani, P., Stalin, C. S., & Goswami, K. D. 2019, MNRAS, 484, 5113
Reimer, A., Böttcher, M., & Buson, S. 2019, ApJ, 881, 46
Ricci, C., & Trakhtenbrot, B. 2023, NatAs, 7, 1282
Ricci, C., Trakhtenbrot, B., Koss, M. J., et al. 2017, ApJS, 233, 17
Rosas, V. G., Isbell, J. W., Jaffe, W., et al. 2022, Natur, 602, 403
Sahakyan, N. 2018, ApJ, 866, 109
Sahu, S., López Fortìn,, C. E., & Nagataki, S. 2020, ApJ, 898, 103
Serafinelli, R., De Rosa, A., Tortosa, A., et al. 2024, A&A, 690, A145
Shakura, N. I., & Sunyaev, R. A. 1973, A&A, 24, 337

Stathopoulos, S. I., Petropoulou, M., Vasilopoulos, G., & Mastichiadis, A. 2024, A&A, 683, A225
Tanaka, Y. T., Buson, S., & Kocevski, D. 2017, ATel, 10791, 1
Tjus, J. B., Jaroschewski, I., Ghorbanietemad, A., et al. 2022, ApJL, 941, L25
Urry, C. M., & Padovani, P. 1995, PASP, 107, 803
Wang, J.-M., Songsheng, Y.-Y., Li, Y.-R., Du, P., & Yu, Z. 2020, MNRAS, 497, 1020
Wang, K., Liu, R.-Y., Li, Z., Wang, X.-Y., & Dai, Z.-G. 2022, Univ, 9, 1
Wang, Z.-J., Liu, R.-Y., Wang, Z.-R., & Wang, J. 2024, ApJ, 962, 142
Winter, W., Gao, S., Rodrigues, X., et al. 2019, in 36th International Cosmic Ray Conf. (ICRC2019) (Trieste: Sissa), 1032
Xue, R., Liu, R.-Y., Petropoulou, M., et al. 2019, ApJ, 886, 23
Yang, Q.-R., Liu, R.-Y., & Wang, X.-Y. 2025, ApJ, 980, 255
Yuan, W., Fausnaugh, M. M., Hoffmann, S. L., et al. 2020, ApJ, 902, 26
Yüksel, H., Kistler, M. D., Beacom, J. F., & Hopkins, A. M. 2008, ApJ, 683, L5
Zhang, B. T., Petropoulou, M., Murase, K., & Oikonomou, F. 2020, ApJ, 889, 118
Zhu, S. F., Brandt, W. N., Luo, B., et al. 2020, MNRAS, 496, 245